Composite Structures 277 (2021) 114619

Contents lists available at ScienceDirect

Composite Structures

journal homepage: www.elsevier.com/locate/compstruct

Shear behavior of green concrete beams reinforced with basalt FRP bars and stirrups

Abathar Al-Hamrani, Wael Alnahhal *, Ayman Elahtem

Department of Civil and Architectural Engineering, Qatar University, Qatar

ARTICLE INFO

Keywords:
Shear behavior
BFRP bars
Green concrete
Fly ash
Silica fume
Analytical analysis

ABSTRACT

This study investigated the shear performance of large-scale green concrete (GC) beams reinforced with basalt fiber reinforced polymer (BFRP) bars and stirrups. The GC concept was employed in this study by partially substituting the cement content with 35% by weight of industrial by-products (fly ash and silica fume). The main test variables were the reinforcement ratio, the shear span to depth ratio (a/d), and the spacing between stirrups. Three beams were transversely reinforced with steel stirrups to serve as a control. Experimental results indicated that the ultimate shear capacity was significantly increased at higher reinforcement ratios. Such effect was less pronounced in beams with reduced spacing between stirrups. In addition, the BFRP stirrups were effective in reducing the diagonal shear crack width and increasing the ultimate shear capacities of the tested beams. On the other hand, beams with a higher a/d ratio have shown higher deflection and reduced ultimate shear capacity. Comparing the experimental results of the current study with the current design codes and guidelines provisions, the CSA-S806-12 has shown the best predictions with a mean experimental to predicted shear (V_{exp}/V_{pre}) ratio of 1.43 ± 0.29.

1. Introduction

There is a growing motivation from researchers and construction practitioners towards the implementation of FRP composites as an alternative to conventional steel reinforcement [1–3]. Keeping in mind that the corrosion in steel is one of the main reasons behind the deterioration of reinforced concrete (RC) structures [4], the use of anti-corrosive FRP bars can play a crucial role in addressing the corrosion issue in RC structures. Nowadays, basalt FRP (BFRP) bars are gaining more popularity in the literature due to their lower price than carbon FRP bars, and their comparable mechanical features to the glass FRP (GFRP) bars [5–10]. Moreover, BFRP bars have shown better thermal resistance compared to GFRP bars [11]. The shear behavior of RC beams reinforced with GFRP bars and stirrups has been well documented in the literature [12–17]. However, a few studies have investigated the shear behavior of RC beams reinforced with BFRP bars [2,18,19]. For instance, Tomlinson and Fam [20] demonstrated that for BFRP-RC beams without stirrups, the shear strength has increased by 39.7% as the reinforcement ratio went from 0.39% to 0.84%, whereas it was increased by 47% with stirrups. Likewise, Issa et al. [2] also noted that the BFRP-RC beams with BFRP stirrups exhibited much higher shear capacity than beams with no BFRP stirrups. However, their effect was less pronounced at higher reinforcement ratios. They also observed a significant increase in the shear capacity of 32% when the reinforcement ratio was increased from 0.8 to 1.3%.

On the other hand, one of the most appealing approaches to have sustainable structures is the use of environmentally friendly green concrete (GC), knowing that concrete is the most used material in the construction sector [21–25]. Meanwhile, Portland cement (PC), one of the main ingredients of concrete, contributes 8% of the global CO_2 emissions [26,27]. Consequently, numerous studies were conducted to examine the feasibility of mitigating the PC consumption through the partial replacement with supplemental cementitious materials such as fly ash (FA) and silica fume (SF) to make GC [28–39]. Both FA and SF are efficient pozzolans which are capable of generating less permeable and denser microstructure than that of PC through the pozzolanic reaction with the hydrated lime and water [31,33]. Nochaiya et al. [40] investigated the impact of utilizing 5% SF with 10% FA replacement on concrete compressive strength and concluded that it was greater than control concrete with 100% PC. Lam et al. [41] stated that replacing the PC by 15% to 25% of FA had shown beneficial effects on the tensile strength of concrete. Arezoumandi et al. [42] investigated the shear

* Corresponding author.
E-mail addresses: aa1205725@qu.edu.qa (A. Al-Hamrani), wael.alnahhal@qu.edu.qa (W. Alnahhal), ae1203787@qu.edu.qa (A. Elahtem).

https://doi.org/10.1016/j.compstruct.2021.114619
Received 27 June 2021; Accepted 30 August 2021
Available online 3 September 2021

strength of RC beams made with a high volume of FA (70% replacement). Their findings revealed an 8 to 12% improvement in shear capacity over standard RC beams. In contrast, experimental results reported by Rao et al. [43] showed a slightly lower shear capacity of RC beams with 50% replacement of FA than the control beam with no added FA.

Combining FRP bars and green concrete is a viable approach to produce sustainable RC structures which have more resistant to weather and chemical exposures. However, researchers have not yet evaluated the structural behavior of GC beams reinforced with FRP bars and stirrups, where supplementary cementitious materials (SCMs) like FA and SF are employed to partially replace the PC. Further research is thus necessary to discover the similarities or differences between the BFRP-GC beams and the traditional ones so that the construction industry may adopt them. Hence, the purpose of this research is to investigate the shear behavior of sand-coated (SC) BFRP bars and stirrups embedded in large-scale GC beams, where cement is partially substituted by FA and SF. Conducting such a study will help provide a better understanding and create new knowledge on the shear design of RC structures using unconventional sustainable materials.

2. Experimental program

2.1. Materials

2.1.1. Concrete mix

The concrete mix proportions for this study are listed in Table 1. Prior to testing, several trial mixes were made in order to achieve 40 MPa compressive strength. The concept of GC was adopted through the partial substitution of cement with industrial by-products namely, SF and FA. The optimum replacement level to achieve the targeted strength was determined to be 35% of the total cement content. After casting of concrete in 200 × 100 mm cylinders, the prepared samples were cured for 28 days and tested in accordance with the provisions of ASTM C39/C39M-20 [44]. The average value of five samples was selected as the representative compressive strength. Similarly, the flexural strength was also determined by testing five 100 × 100 × 500 mm prisms in accordance with the provisions of ASTM C1609/C1609M-12 [45]. The compressive and flexural strengths were determined to be 44.5 MPa and 4 MPa, respectively, as shown in Table 2.

2.1.2. BFRP bars and stirrups

Two BFRP bar diameters of 12 and 16 mm were used to reinforce the large-scale beams, as shown in Fig. 1a. The mechanical properties of BFRP bars were determined in accordance with ASTM D7205/D7205M-06 [46] provisions, using the universal testing machine (UTM). Five bars have been chosen randomly from each bar diameter. The obtained tensile strength and modulus of elasticity for both bar diameters are listed in Table 3. As shown in Fig. 1b, a BFRP stirrups of size 10 mm with an ultimate tensile strength of 1000 MPa and modulus of elasticity of 50 GPa, as provided by its manufacturer [47], were used to reinforce the beams against shear. The surface of the BFRP bars and the stirrups were sand coated to enhance their bonding behavior with the surrounding concrete.

Table 1
Concrete mix proportions.

Materials	Mix proportion (Kg/m^3)
Cement	260
SF	80
FA	60
20 mm Limestone	481
10/14 mm limestone	633
Sand	750
Superplasticizers	4.5
Water	149

Table 2
Compressive and flexural test results.

Specimen No.	Flexural Strength (MPa)	Avg. Flexural Strength (MPa)	Compressive Strength (MPa)	Avg Compressive Strength (MPa)
1	4.2	4.0	45.23	44.5
2	3.42		41.63	
3	4.53		44.72	
4	3.45		45.68	
5	4.53		45.42	

2.1.3. Large-scale beams

In this study, 14 GC beams were longitudinally and transversely reinforced with SC-BFRP bars and stirrups. The beams were loaded at two shear spans to depth ratios of 2.5 and 3.5. To evaluate the dowel action of the longitudinal BFRP bars, two reinforcement ratios were used above the balanced reinforcement ratio (ρ_b) as 2.54$\rho_b$and 4.5ρ_b, as per ACI 440.1R-15 [48] recommendations. The BFRP stirrups were placed at two spacings of 250 and 350 mm. Three beams were reinforced with steel stirrups to serve as control beams, while another three beams have no stirrups to better evaluate the contribution of BFRP stirrups to shear strength. The detailed testing matrix is shown in Table 4. The first letter in the beam designation represents the type of stirrups, where "B" refers to basalt, "G" refers to glass, and "NS" refers to beams with no stirrups. The following lower case $\boldsymbol{\rho}$ refers to the bottom longitudinal reinforcement ratio, where ρ_1 is equivalent to 2.54ρ_b, and ρ_2 is equivalent to 4.5ρ_b. The number of 2.5 or 3.5 is referred to the shear span to depth ratio, while the number of 250 or 350 is referred to the distances between stirrups.

2.1.4. Instrumentation and test procedure

The large-scale beams dimensions were 200 × 300 × 2550 mm, as shown in the schematic drawing in Fig. 2. All beams were subjected to four-point loading until failure with a loading rate of 1 mm/min. The midspan deflection was recorded through a linear variable differential transformer (LVDT). At the midspan, one strain gauge was placed on the top of the beam to measure concrete strain, whereas another strain gauge was placed below the bottom reinforcement to measure the BFRP bar strain. The diagonal shear crack width was measured by a crack transducer placed at the mid shear span. The concrete clear cover on all sides was 30 mm. Additionally, 2ϕ10 BFRP bars were used as a compression reinforcement in all beams. The reinforcement arrangement and beam configuration are shown in detail in Fig. 2.

3. Test results and discussions

Table 5 provides the maximum applied load, midspan deflection, strain in both concrete and BFRP bars, and cracking load of the tested beams.

3.1. Load-deflection response

The applied load versus midspan deflection relationships are shown in Fig. 3. Initially, all beams revealed linear behavior prior to the onset of flexural cracking. Regardless of the cracking load capacity, all beams were cracked approximately at similar deflection. The point of loading where each beam experienced the first crack was highly associated with the a/d ratio. By referring to Table 5, beam B-ρ_2-3.5–250 with a/d = 3.5 cracked at a cracking moment (M_{cr}) of 38 kN.m, whereas beam B-ρ_2-2.5–250 with a/d = 2.5 cracked at M_{cr} of 54 kN.m. After cracking, the load–deflection behavior for the tested beams remains linear but at a steeper slope. This is attributed to the development of several flexural cracks along the clear span, which increased in depth as the applied load was increased, thus reducing the moment of inertia. Similar to conventional concrete beams, Fig. 3 shows that GC beams with a higher

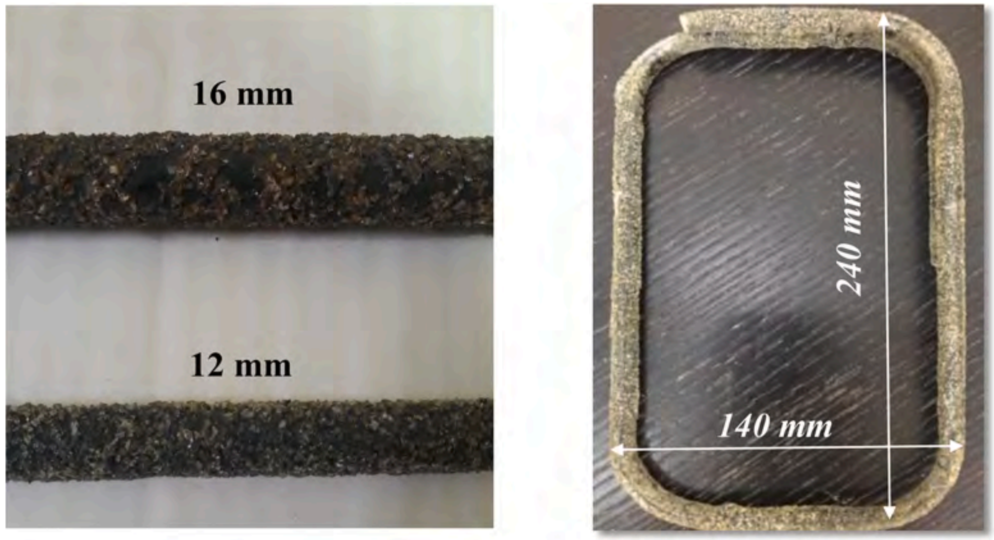

(a) (b)

Fig. 1. Reinforcing elements used in this study: (a) BFRP bars; (b) BFRP stirrups.

Table 3
Material properties for the used BFRP bars.

Material Properties	SC-BFRP bars	
Diameter of the bar (mm)	16	12
Tensile Strength (MPa)	1110	1177
Ultimate strain %	2.38	2.55
Elastic Modulus (GPa)	46.51	49.48

reinforcement ratio or lower a/d ratio have exhibited higher stiffness along the entire post-cracking stage. As an example, at the failure load of beam B-ρ_1-2.5–250, beam B-ρ_2-2.5–250 showed less deflection by 34.6%, while the deflection was reduced by 53.8% in beam B-ρ_1-2.5–350 at the failure load of beam B-ρ_1-3.5–350. The ultimate deflection value, however, was observed not to be affected by the different a/d ratios. Furthermore, Fig. 3 illustrates that the load–deflection responses for beams with 250 mm spacing between stirrups followed the same trend as their counterpart beams with 350 mm. However, the main difference was in their ultimate deflections and loading capacities as beams with 250 mm stirrups spacing failed at a higher loading level, which was expected due to the presence of more stirrups along the shear span. Fig. 3 also shows that the control beams with steel stirrups compared to beams with BFRP stirrups resulted in higher ultimate loading capacity and stiffness along the post cracking stage due to the higher axial stiffness and better confinement of steel stirrups than the BFRP ones.

3.2. Load-strain response

Fig. 4 compares the load versus midspan strain values for concrete and longitudinal BFRP bars. It was clear that beams with higher reinforcement ratios have encountered less strain values for both concrete (Fig. 4a) and BFRP bars (Fig. 4b). As shown in Fig. 4b, at a loading point of 55 kN, the strain in BFRP bars for beam B-ρ_2-3.5–350 was 63.9% less than beam B-ρ_1-3.5–350. Furthermore, strain values increased at a higher rate after cracking; however, this increase was mitigated when a higher reinforcement ratio or less a/d ratio was used. Also, at the ultimate shear capacity of beam B-ρ_2-3.5–250 with a/d = 3.5, the beam B-ρ_2-2.5–250 with a/d = 2.5 have shown 49% and 44% less strain in BFRP bars and concrete, respectively. This was expected due to the longer moment arm at higher a/d ratio, which induced higher midspan deflection. Thus, this resulted in higher compressive stress on the top concrete on one side and higher stretching effect on the bottom BFRP bars from the other [18]. Furthermore, the reference beams with steel

Table 4
Testing matrix.

Beam designation	Reinforcement ratio ρ/ρ_b	No. and diameter of BFRP bars	a/d ratio	Spacing between stirrups (mm)	Type of the stirrups
B-ρ_1-2.5–250	2.54	6ϕ12	2.5	250	BFRP
B-ρ_1-2.5–350	2.54	6ϕ12	2.5	350	BFRP
B-ρ_1-3.5–350	2.54	6ϕ12	3.5	350	BFRP
B-ρ_1-3.5–250	2.54	6ϕ12	3.5	250	BFRP
B-ρ_2-3.5–250	4.5	5ϕ16	3.5	250	BFRP
B-ρ_2-2.5–250	4.5	5ϕ16	2.5	250	BFRP
B-ρ_2-2.5–350	4.5	5ϕ16	2.5	350	BFRP
B-ρ_2-3.5–350	4.5	5ϕ16	3.5	350	BFRP
S-ρ_1-2.5–250	2.54	6ϕ12	2.5	250	Steel
S-ρ_1-2.5–350	2.54	6ϕ12	2.5	350	Steel
S-ρ_2-2.5–250	4.5	5ϕ16	2.5	250	Steel
NS-ρ_2-3.5	4.5	5ϕ16	3.5	–	No-stirrups
NS-ρ_2-2.5	4.5	5ϕ16	2.5	–	No-stirrups
NS-ρ_1-2.5	2.54	6ϕ12	2.5	–	No-stirrups

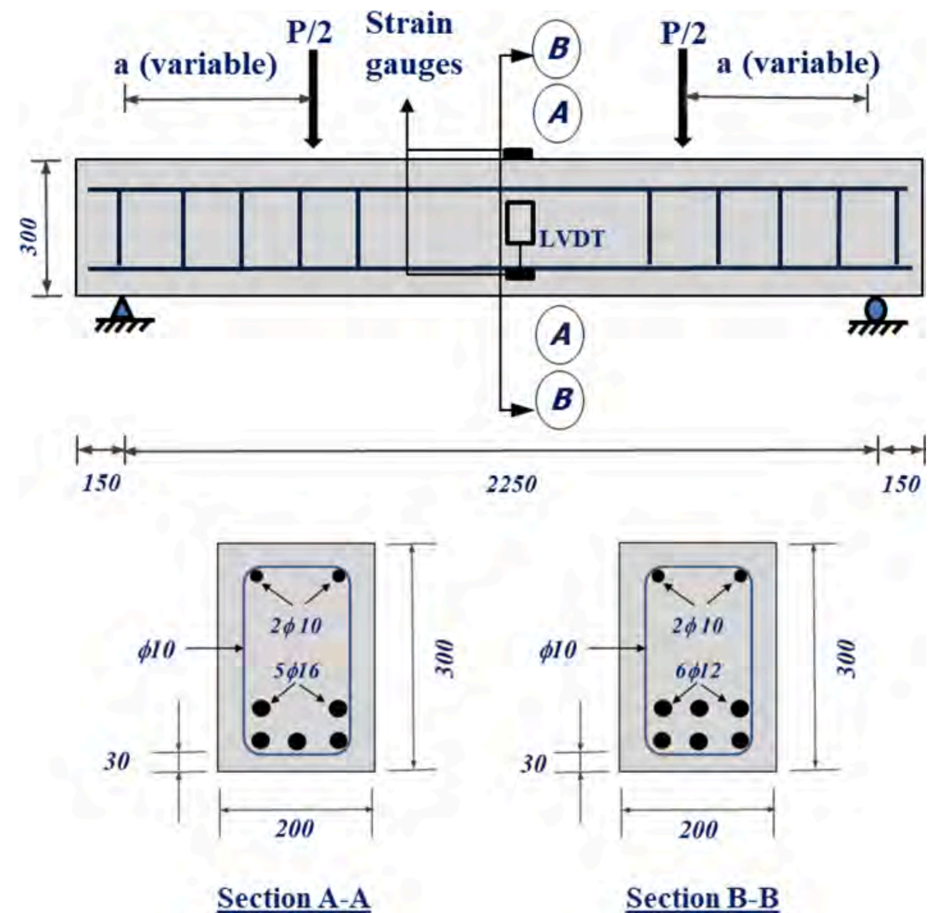

Fig. 2. Beams test setup (All dimensions are in mm).

Table 5
Summary of test results.

Beam designation	Max. load P/2 (kN)	Δ_{Max} (mm)	Max. strain FRP	Max. strain concrete	M_{cr} (kN.m)	Failure type	Angle of failure
B-ρ_1-2.5–250	119.7	35.12	0.0086	0.002	41	DT	45
B-ρ_1-2.5–350	70.76	18.1	0.0053	0.001	47	DT	48
B-ρ_1-3.5–350	57.66	20.26	0.0075	0.0017	45	DT	44
B-ρ_1-3.5–250	89.85	34.07	0.012	0.0034	34	SC	40
B-ρ_2-3.5–250	92.65	28.2	0.008	0.0027	38	SC	38
B-ρ_2-2.5–250	123.79	28	0.0074	0.0026	54	DT	35
B-ρ_2-2.5–350	87.5	19.1	0.006	0.0016	45	DT	43
B-ρ_2-3.5–350	65.75	20.24	0.005	0.0017	27	DT	45
S-ρ_1-2.5–250	142.2	39.7	0.012	0.00275	51	CF	–
S-ρ_1-2.5–350	90.3	20.88	0.0062	0.00145	59	DT	45
S-ρ_2-2.5–250	142.2	32.1	0.0083	0.0027	58	SC	38
NS-ρ_2-3.5	54.68	12.8	0.004	0.0013	40	DT	40
NS-ρ_2-2.5	88.39	16.82	0.0045	0.0017	43	DT	48
NS-ρ_1-2.5	61	10.6	0.0041	0.00135	49	DT	45

Δ_{Max} = Maximum deflection; M_{cr} = Cracking moment; DT = Diagonal tension failure; SC = Shear compression failure; CF = Compression flexural failure.

stirrups experienced higher ultimate strain values for concrete and BFRP bars than the counterpart beams with BFRP stirrups due to their higher ultimate loading capacities. For instance, the ultimate concrete and BFRP bar strains in the reference beam S-ρ_1-2.5–250 were recorded as 37.15 and 22.0% higher than beam B-ρ_1-2.5–250. Moreover, it is apparent from Fig. 4 that beams without stirrups demonstrated low strain values because of their failure at earlier loading levels than their counterpart beams with stirrups.

3.3. Crack patterns and failure modes

The crack patterns and the failure modes of the tested beams are presented in Fig. 5. The first flexural crack was vertically formed at the maximum moment zone. Additional flexural cracks were noticed to develop in the same zone and along the two shear spans at higher load application. For cracks in the shear span, as their penetration depth was increasing, the cracks demonstrated progressive inclination toward the loading point due to the dominance of the shear stress at this zone. All

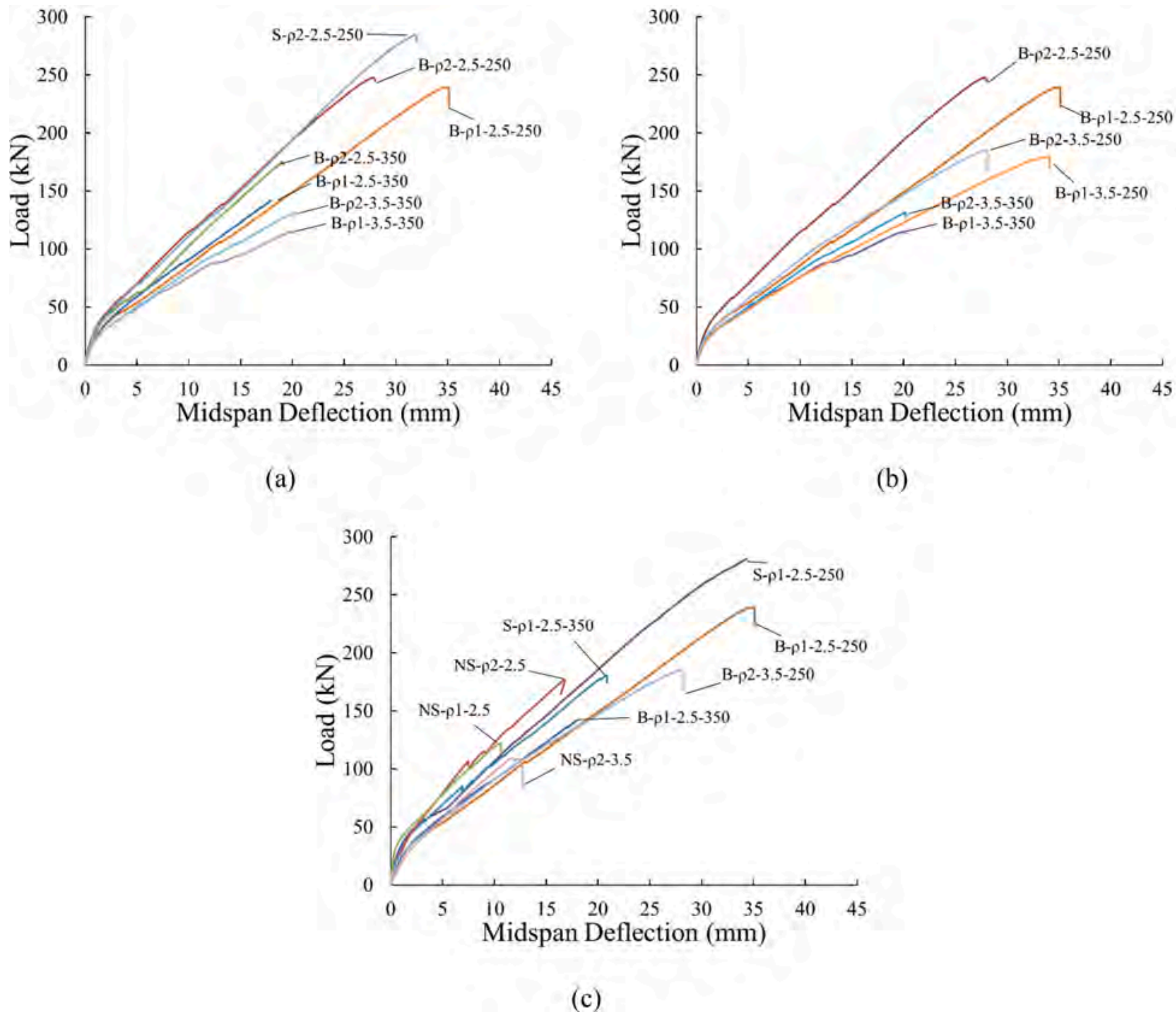

Fig. 3. Load vs. midspan deflection.

beams have experienced diagonal tension (DT) failure, except four beams which had either a shear compression failure (SC) or a compression flexural (CF) failure. While beam B-ρ_1-2.5–250 with a/d = 2.5 had DT failure, the increased a/d of 3.5 in beam B-ρ_1-3.5–250 has led to SC failure, which comprises crushing of concrete at first, followed by major diagonal shear crack. Likewise, the failure in beams B-ρ_2-2.5–250 and B-ρ_2-3.5–250 were DT and SC, respectively. The crushing of concrete could be related to the formation of higher compressive stresses at the compression side, which were induced from the longer a/d ratio. The reference beam S-ρ_2-2.5–250 noticed to delay the formation of major shear crack from 123.8 kN in beam B-ρ_2-2.5–250 to 142.2 kN, and converted the failure mode from DT into SC. Furthermore, although shear cracks were developed in the reference beam S-ρ_1-2.5–250, as shown in Fig. 5, the steel stirrups had interestingly prevented their widening and changed the failure mode into CF failure. This could be attributed to the higher modulus of elasticity of steel and its better bonding characteristics with the surrounding concrete than the BFRP stirrups.

3.4. Load vs. Shear crack response

The diagonal shear crack responses against the applied load are presented in Fig. 6. According to the figure, increasing the reinforcement ratio from $2.54\rho_b$ to $4.5\rho_b$resulted in a considerable reduction in crack width. At failure of beam B-ρ_1-2.5–250, the crack width was 3.39 mm, while it was 1.5 mm in B-ρ_2-2.5–250. Furthermore, the lesser spacing between stirrups have also reduced the crack width in beam B-ρ_2-2.5–250 from 1.47 mm in beam B-ρ_2-2.5–350 to 0.72 mm. The crack width in beam S-ρ_2-2.5–250 with steel stirrups was 0.65 mm; whereas, it was 1.5 mm in beam B-ρ_2-2.5–250 with BFRP stirrups. This could be attributed to the greater axial stiffness of steel compared to BFRP stirrups. Another observation to emerge from Fig. 6 that the shear crack width was significantly reduced due to the presence of BFRP stirrups. At a loading point of 175 kN, the shear crack width in beam NS-ρ_2-2.5 with no stirrups was recorded to be 2.13 mm, whereas it was recorded to be 1.47 and 0.72 mm in beams B-ρ_2-2.5–350 and B-ρ_2-2.5–250 with stirrups spacing of 350 and 250 mm, respectively.

3.5. Load-carrying capacity

Table 5 shows the load-carrying capacity of each beam. In the light of these results, it was observed that as the spacing between stirrups was reduced, the reinforcement ratio contribution to the ultimate shear capacity was almost diminished. This correlation can be demonstrated by the comparison between beams NS-ρ_1-2.5 and NS-ρ_2-2.5 with no stirrups, which results in a 44% difference in the ultimate shear capacity, while the difference was reduced to 14 and 23.7% for beams B-ρ_1-3.5–350 and B-ρ_1-2.5–350 compared to beams B-ρ_2-3.5–350 and B-

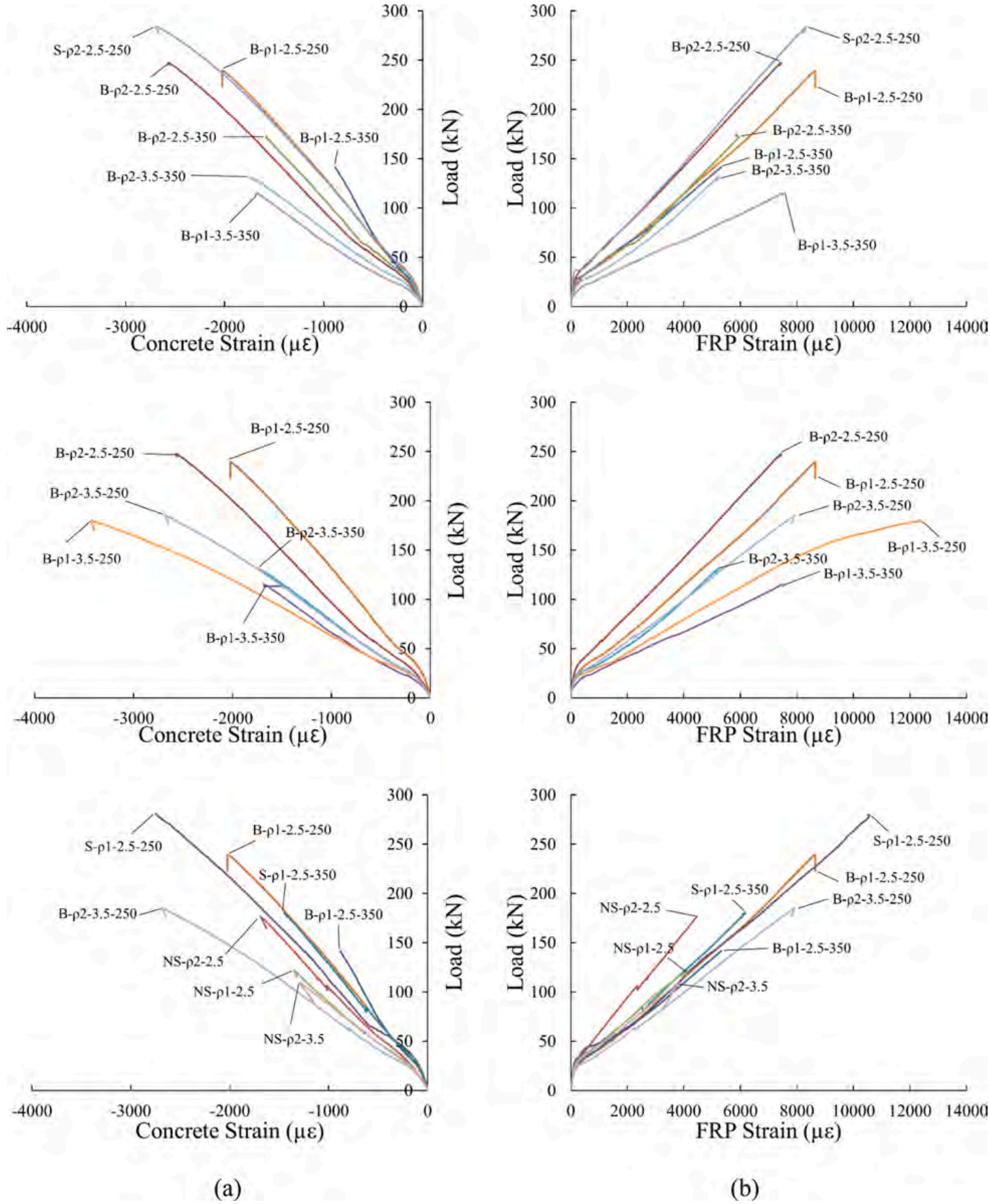

Fig. 4. Load vs. midspan strain: (a) Concrete strain; (b) FRP strain.

ρ_2-2.5–350, respectively. Interestingly, this difference was further reduced to 3% at a lower spacing of 250 mm by comparing beams B-ρ_1-3.5–250 and B-ρ_2-3.5–250. The presence of more stirrups provided a significant contribution to the ultimate shear capacity compared to the contribution of longitudinal bars, which may explain why the reinforcement ratio impact was less evident at the smaller spacing between stirrups.

In addition, The results, as shown in Fig. 3a and b, indicate that the lower the a/d ratio, the higher the ultimate shear capacity. For example, beam B-ρ_2-2.5–350 shows 33% gain in shear capacity compared to beam B-ρ_2-3.5–350. Furthermore, as shown in Fig. 3a and b, the beams group with 250 mm spacing between stirrups demonstrated 40 to 69% higher shear capacity than those with stirrups spacing of 350 mm. This clearly reflects the effectiveness of BFRP stirrups in preventing the formation of major diagonal shear cracks. As anticipated, the control beams with steel stirrups contributed more to shear strength than their counterpart beams

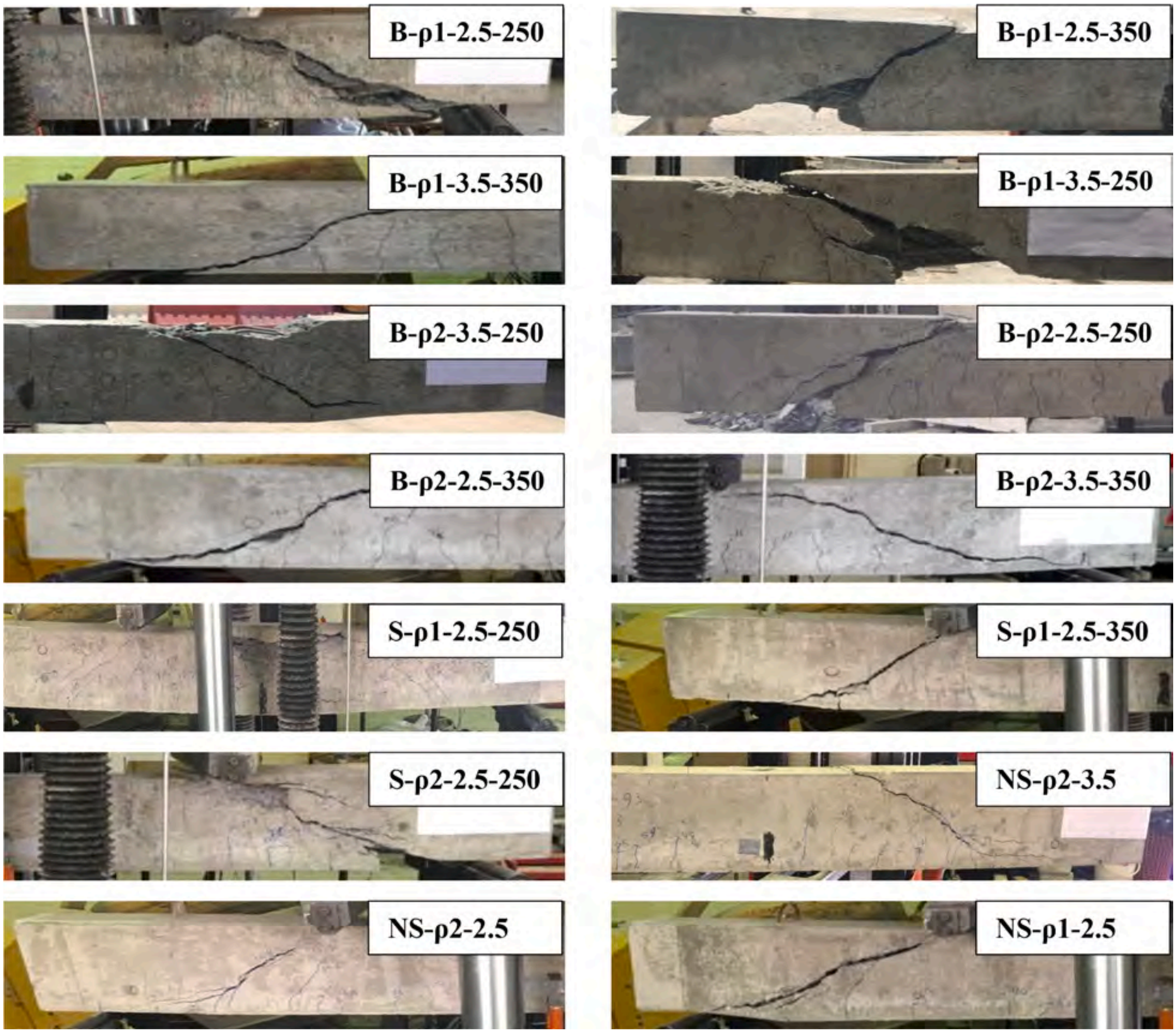

Fig. 5. Crack patterns of the tested beams.

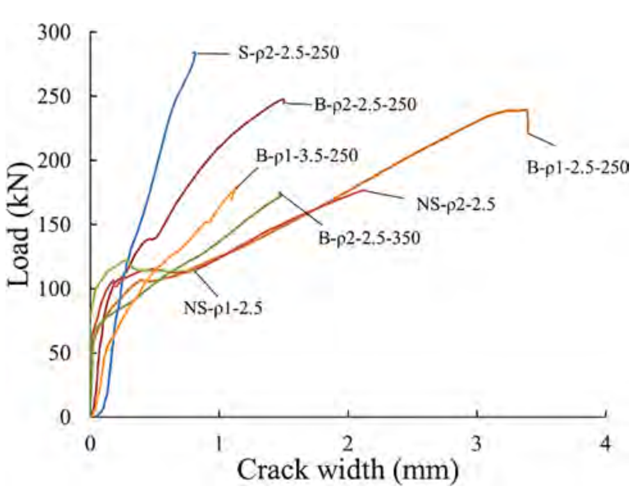

Fig. 6. Load vs. diagonal shear crack width.

with BFRP stirrups. This difference was 27.6% for beams with 350 mm stirrups spacing, whereas it was in the range of 14.8 to 18.8% for beams with 250 mm spacing. By comparing the BFRP stirrups reinforced beams with those without stirrups, it can be concluded that the BFRP stirrups were very effective in contributing to the shearing strength. As an example, beams B-ρ_1-2.5–250 and B-ρ_2-3.5–250 have shown a significant increase in ultimate shear capacity of 96.2% and 69.4% over beams NS-ρ_1-2.5 and NS-ρ_2-3.5, respectively, as shown in Fig. 3c.

4. Predictions of shear capacities

Four current shear design guidelines and codes were utilized to determine which of them might be used to estimate the shear capacity of the proposed BFRP-GC beams. In this section, the experimental shear capacities of the tested beams were compared against the following FRP design guidelines: ACI 440.1R-15 [48], the CSA-S806-12 [49], the ISIS 2007 [50], and the JSCE-97 [51]. The detailed shear equations are listed in Table 6, which shows that the concrete and the FRP stirrups' contribution to the shearing strength are calculated independently. The experimental versus the predicted shear capacities are summarized in Table 7 and plotted in Fig. 7. It can be seen from the data in Table 7 and Fig. 7 that all the aforementioned design guidelines have conservatively predicted the experimental results. However, the equations of the CSA-S806-12 [49] reported more accurate predictions of the shear capacities than the other three shear models. For instance, the mean experimental to predicted shear capacities (V_{exp}/V_{pre}) ratio of the CSA-S806-12 [49]

Table 6
The analytical models.

Design code/ guideline	Concrete contribution, Vc (N)	Stirrups contribution, V_{frp} (N)
ACI 440.1R-15 [48]	$V_c = \frac{2}{5}\sqrt{f'c}\,b_w k d$ (1) $k = \sqrt{2\rho n + (\rho n)^2} - \rho n$ b_w = beam width d = beam effective depth n = ratio of modulus of elasticity of FRP bars to modulus of elasticity of concrete	$V_{frp} = \frac{A_{fv} f_{fv} d}{s}$ (2) A_{fv} = area of FRP shear reinforcement within spacing s, (mm^2) f_{fv} = tensile strength of FRP taken as the smallest of design tensile strength f_{fu}, strength of bent portion of FRP stirrupsf_{fb}, or stress corresponding to $0.004E_f$, (MPa). Where $f_b = \left(0.05\left(\frac{rb}{db}\right) + 0.3\right)f_{fuv}$
CSA-S806-12 [49]	$V_c = 0.05\lambda k_m k_r (f'c)^{\frac{1}{3}} b_w d_v$, for $d \le 300$ mm (3) where $0.11\sqrt{f'c}\,b_w d_v \le V_c \le 0.22\sqrt{f'c}\,b_w d_v$ $k_m = \sqrt{\frac{V_f d}{M_f}1.0}$, where $\left(\frac{V_f d}{M_f}\right)$ is equivalent to $\left(\frac{d}{a}\right)$ $k_r = 1 + (E_f\rho)^{\frac{1}{3}}$	$V_{frp} = \frac{A_{fv} f_{fu} d_v}{s}\cot\theta$ (4) $f_{fu} \le 0.005E_f$ $\theta = 30^o + 7000\varepsilon_l$ provided that $30^o \le \theta \le 60^o$ $\varepsilon_l = \frac{\frac{M_f}{d_v} + V_f + 0.5N_f}{E_f A_{FV}}$
ISIS 2007 [50]	$V_c = 0.2\lambda\sqrt{f'c}\,b_w d\sqrt{\frac{E_f}{E_s}}$ (5) E_s = Elastic modulus for steel E_f = Elastic modulus for FRP	$V_{frp} = \frac{A_{fv} f_{fv} d_v \cot\theta}{s}$ (6) $f_{fv} = \frac{\left(0.05\left(\frac{rb}{db}\right) + 0.3\right)f_{fuv}}{1.5}$, or $f_{fv} = E_{fv}\varepsilon_{fwd}$ $d_v = 0.9d$ θ = angle of inclination of shear plane assumed as 45^o $\varepsilon_{fwd} = 0.0001\left(f'_c\left(\frac{\rho E_f}{\rho_w E_{fv}}\right)\right)^{\frac{1}{2}}$ (7)
JSCE-97 [51]	$V_c = \beta_d\beta_p\beta_n f_{vcd} b_w d/\gamma_b$ (8) $\beta_d = \left(\frac{1000}{d}\right)^{\frac{1}{4}} \le 1.5$ $\beta_p = \left(\frac{1000\rho E}{E_s}\right)^{\frac{1}{4}} \le 1.5$ $\beta_n = 1$ if no axial force apllied $f_{vcd} = 0.2\sqrt[3]{f'c}$ provided that $f_{vcd} \le 0.72\frac{N}{mm^2}$ $\gamma_b = 1.3$	$V_{frp} = [A_{fv} E_{fv}\varepsilon_{fwd}(\cos\alpha_s + \sin\alpha_s)/s]z/\gamma_{bs}$ (9) α_s = angle formed by shear reinforcement and member axis $z = \frac{d}{1.15}$ $\gamma_{bs} = 1.15$ $\varepsilon_{fwd} = 0.0001\left(f'_{mcd}\left(\frac{\rho E_f}{\rho_w E_{fv}}\right)\right)^{\frac{1}{2}}[1 + 2\left(\frac{\sigma_n}{f'_{mcd}}\right)]$ $\rho_w = A_{fv}/b_w s$ $f'_{mcd} = \left(\frac{h}{0.3}\right)^{-\frac{1}{10}} f'c$

was 1.43 ± 0.29 with the least coefficient of variation COV% of 20.54. On the other hand, the ACI-440–15, the ISIS-2007, and the JSCE-97 have shown more conservative predictions with mean V_{exp}/V_{pre} = 1.97 ± 0.53, 2.28 ± 0.59, and 1.91 ± 0.43 and COV% of 26.98, 26.09, and 22.75, respectively.

The effect of the test variables (stirrups spacing, a/d ratio, and the reinforcement ratio) on the V_{exp}/V_{pre} ratio are also shown in Fig. 7. In general, Fig. 7 illustrates that all shear models resulted in more accurate predictions for beams having 350 mm spacing between stirrups than those having 250 mm. Likewise, the predictions were noticed to be more accurate at a longer a/d ratio. While the existing literature has recognized the critical role of both a/d ratio and the reinforcement ratio on the shear strength [2,5,14–17,20,52], the current FRP design guidelines have underestimated their effect. In the current study, it was reported in the previous section that reducing the a/d from 3.5 to 2.5 resulted in 33% higher shear capacity. However, as shown in Table 7 and Fig. 7, the ACI 440.1R-15 [48], ISIS 2007 [50], and JSCE-97 [51] do not account for the a/d effect, and therefore, similar predictions were recorded for counterpart beams with different a/d ratios. This can help to justify the highly conservative predictions obtained from these design guidelines. On the other hand, CSA-S806-12 [49] accounts for the a/d effect, where the predicted shear capacity was increased by13% when reducing the a/d from 3.5 to 2.5.

Contrary to expectations, the predicted concrete shear capacities by ISIS 2007 [50] were decreased as the reinforcement ratio was increased. This is because the main reinforcement effect was incorporated in by ISIS 2007 [50] in terms of E_f, where the reported values of $E_f$in this study were 49.48 and 46.51 GPa for the 12 and 16 mm bar diameters, respectively. This is another source of inaccuracy that can clearly illustrate why ISIS 2007 [50] guidelines had the least accurate predictions of the shear capacities of the tested beams. However, based on the experimental results, it appears that the current FRP design guidelines and codes may be utilized to design BFRP-GC beams for shear because the experimental results were conservatively expected. Further research, however, should be conducted to validate this premise using different parameters impacting the shear capacities of BFRP-RC beams.

5. Conclusions

This study investigated the shear behavior of BFRP–RC beams, where the cement content was partially replaced with FA and SF. The results of this investigation have demonstrated that:

Table 7
The experimental vs predicted shear capacities of the tested beams.

Beam designation	Experimental shear (kN)	ACI-440-15 [48]		CSA-S806-12 [49]		ISIS-2007 [50]		JSCE-97 [51]	
		V_{pre}, kN	V_{exp}/V_{pre}	V_{pre}, kN	V_{exp}/V_{pre}	V_{pre}, kN	V_{exp}/V_{pre}	V_{pre}, kN	V_{exp}/V_{pre}
B-ρ_1-2.5–250	119.7	54.33	2.20	67.2	1.78	41.25	2.90	43.40	2.76
B-ρ_1-2.5–350	70.8	45.74	1.55	62.8	1.13	39.78	1.78	41.97	1.69
B-ρ_1-3.5–350	57.7	45.74	1.26	54.6	1.06	39.78	1.45	41.97	1.37
B-ρ_1-3.5–250	89.9	54.33	1.65	59.8	1.50	41.25	2.18	43.40	2.07
B-ρ_2-3.5–250	92.7	57.78	1.60	63.6	1.46	41.70	2.22	48.86	1.90
B-ρ_2-2.5–250	123.8	57.78	2.14	71.7	1.73	41.70	2.97	48.86	2.53
B-ρ_2-2.5–350	87.5	49.27	1.78	69.3	1.26	39.96	2.19	47.19	1.85
B-ρ_2-3.5–350	65.8	49.27	1.34	61.6	1.07	39.96	1.65	47.19	1.39
S-ρ_1-2.5–250	142.2	*	*	*	*	*	*	*	*
S-ρ_1-2.5–350	90.3	45.74	1.97	61.6	1.47	39.78	2.27	55.64	1.62
S-ρ_2-2.5–250	142.2	57.78	2.46	71.7	1.98	41.70	3.41	67.82	2.10
NS-ρ_2-3.5	54.7	28.00	1.95	44.3	1.24	30.50	1.79	38.04	1.44
NS-ρ_2-2.5	88.4	28.00	3.16	52.4	1.69	30.50	2.90	38.04	2.32
NS-ρ_1-2.5	61	24.29	2.51	47.7	1.28	31.72	1.92	34.19	1.78
Mean			1.97		1.43		2.28		1.91
SD			0.53		0.29		0.59		0.43
COV%			26.98		20.54		26.09		22.75

* Compression flexural failure.

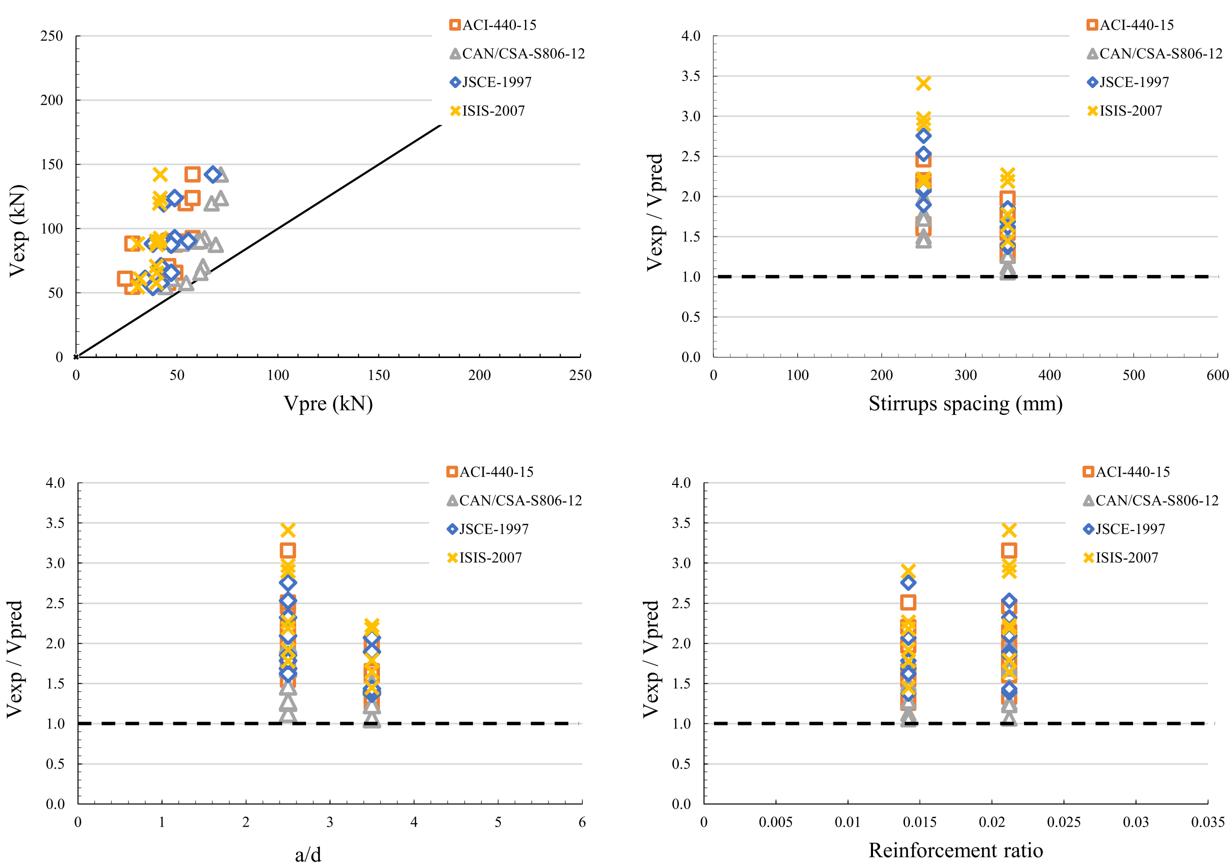

Fig. 7. Experimental vs. predicted shear capacity (Vexp/Vpre) and the effect of stirrups spacing, a/d ratio, and the reinforcement ratio on the prediction accuracy.

- Increasing the reinforcement ratio from $2.54\rho_b$ to $4.5\rho_b$ resulted in a 44% increase in the ultimate shear capacity. However, this enhancement was less pronounced with the presence of stirrups.
- Lesser shear crack widths were reported in beams with higher reinforcement ratio. These beams have also reported 63.9 and 34.6% decrease in the longitudinal BFRP bars strain and the midspan deflection, respectively at the same loading level.
- Decreasing the a/d ratio from 3.5 to 2.5 has increased the ultimate shear capacity by 33% and decreased the midspan deflection by 53.8% at the same loading level. As a result, the strain in BFRP bars and concrete were also noticed to decrease by 49% and 44%, respectively.

- Reducing the spacing of stirrups from 350 mm to 250 mm demonstrated 40% to 69% increase in the ultimate shear capacity, while it was further increased by 96.2% compared to beams with no stirrups.
- The maximum shear capacity in BFRP-RC beams with BFRP stirrups was reduced by 27.6% compared to reference beams with steel stirrups spaced at 350 mm, and by 14.8% to 18.8% for beams with 350 mm stirrups spacing.
- Wider shear cracks were observed in beams reinforced with BFRP stirrups than those reinforced with steel stirrups. This is attributed to the lower elastic modulus of BFRP stirrups compared to steel ones.
- Based on the analytical analysis, the current guidelines and code-based shear design equations have conservatively predicted the experimental shear capacities of the GC beams. The CSA-S806-12 shear equation provided the most accurate predictions of the shear capacities of the tested beams with $V_{exp}/V_{pre} = 1.43 \pm 0.29$. On the other hand, the ACI-440–15, ISIS-2007, and JSCE-97 have shown excessively conservative predictions with $V_{exp}/V_{pre} = 1.97 \pm 0.53$, 2.28 ± 0.59, and 1.91 ± 0.43, respectively.

Declaration of Competing Interest

The authors declare that they have no known competing financial interests or personal relationships that could have appeared to influence the work reported in this paper.

Acknowledgments

The authors show their gratitude to Qatar Foundation for their financial support through the UREP award no. **UREP21-089-2-039** and GSRA grant no. **GSRA6-1-0301-19005** from the Qatar National Research Fund (QNRF, a member of Qatar Foundation). The authors also show their gratitude to Qatar University for their financial support through internal research grants no. **QUST-1-CENG-2021-21**. Also, the authors would like to thank **Galen LLC** for providing the BFRP bars used in this study. Open Access funding provided by the Qatar National Library. The findings achieved herein are solely the responsibility of the authors.

Data availability

The raw/processed data required to reproduce these findings cannot be shared at this time as the data also forms part of an ongoing study.

References

[1] Belarbi A, Acun B. FRP systems in shear strengthening of reinforced concrete structures. Procedia Eng., vol. 57, Elsevier B.V.; 2013, p. 2–8. https://doi.org/10.1016/j.proeng.2013.04.004.
[2] Issa MA, Ovitigala T, Ibrahim M. Shear behavior of basalt fiber reinforced concrete beams with and without basalt FRP stirrups. J Compos Constr 2016;20(4):04015083. https://doi.org/10.1061/(ASCE)CC.1943-5614.0000638.
[3] Aref A, Alnahhal W. Experimental evaluation of a hybrid FRP-concrete bridge superstructure system under negative moment flexural loads. Jordan J Civ Eng 2007;1:336–43.
[4] Fang C, Lundgren K, Chen L, Zhu C. Corrosion influence on bond in reinforced concrete. Cem Concr Res 2004;34(11):2159–67. https://doi.org/10.1016/j.cemconres.2004.04.006.
[5] El Refai A, Abed F. Concrete contribution to shear strength of beams reinforced with basalt fiber-reinforced bars. J Compos Constr 2016;20(4):04015082. https://doi.org/10.1061/(ASCE)CC.1943-5614.0000648.
[6] Attia K, Alnahhal W, Elrefai A, Rihan Y. Flexural behavior of basalt fiber-reinforced concrete slab strips reinforced with BFRP and GFRP bars. Compos Struct 2019;211:1–12. https://doi.org/10.1016/j.compstruct.2018.12.016.
[7] Attia K, Alnahhal W, Elrefai A, Rihan Y. Flexural behavior of basalt fiber-reinforced concrete slab strips reinforced with BFRP and GFRP bars 2019;211:1–12. https://doi.org/10.1016/j.compstruct.2018.12.016.
[8] Abushanab A, Alnahhal W, Farraj M. Structural performance and moment redistribution of basalt FRC continuous beams reinforced with basalt FRP bars. Eng Struct 2021;240:112390. https://doi.org/10.1016/j.engstruct.2021.112390.
[9] Taha A, Alnahhal W. Bond durability and service life prediction of BFRP bars to steel FRC under aggressive environmental conditions. Compos Struct 2021;269:114034. https://doi.org/10.1016/j.compstruct.2021.114034.
[10] Taha A, Alnahhal W, Alnuaimi N. Bond durability of basalt FRP bars to fiber reinforced concrete in a saline environment. Compos Struct 2020;243:112277. https://doi.org/10.1016/j.compstruct.2020.112277.
[11] Sim J, Park C, Moon DY. Characteristics of basalt fiber as a strengthening material for concrete structures. Compos Part B Eng 2005;36(6-7):504–12. https://doi.org/10.1016/j.compositesb.2005.02.002.
[12] Shehata E, Morphy R, Rizkalla S, Shehata Wardrop E, Morphy Crosier Kilgour R, Rizkalla S, et al. Fibre reinforced polymer shear reinforcement for concrete members: behaviour and design guidelines. Can J Civ Eng 2000;27:859–72.
[13] Alkhrdaji T, Wideman M, Belarbi ANA. Shear strength of GFRP RC beams and slabs. In: Figueiras J, Juvandes L, Furia R, Porto P, editor. Proc., 2nd Int. Conf. Compos. Constr., 2001, p. 409–414.
[14] Bentz EC, Massam L, Collins MP. Shear strength of large concrete members with FRP reinforcement. J Compos Constr 2010;14(6):637–46. https://doi.org/10.1061/(ASCE)CC.1943-5614.0000108.
[15] Mahmoud K, El-Salakawy E. Shear strength of GFRP-reinforced concrete continuous beams with minimum transverse reinforcement. J Compos Constr 2014;18(1):04013018. https://doi.org/10.1061/(ASCE)CC.1943-5614.0000406.
[16] Kim CH, Jang HS. Concrete shear strength of normal and lightweight concrete beams reinforced with FRP bars. J Compos Constr 2014;18(2):04013038. https://doi.org/10.1061/(ASCE)CC.1943-5614.0000440.
[17] Said M, Adam MA, Mahmoud AA, Shanour AS. Experimental and analytical shear evaluation of concrete beams reinforced with glass fiber reinforced polymers bars. Constr Build Mater 2016;102:574–91.
[18] Al-Hamrani A, Alnahhal W. Shear behavior of basalt FRC beams reinforced with basalt FRP bars and glass FRP stirrups: experimental and analytical investigations. Eng Struct 2021;242:112612. https://doi.org/10.1016/j.engstruct.2021.112612.
[19] Tomlinson D, Fam A. Performance of concrete beams reinforced with basalt FRP for flexure and shear. J Compos Constr 2015;19(2):04014036. https://doi.org/10.1061/(ASCE)CC.1943-5614.0000491.
[20] Tomlinson D, Fam A. Performance of concrete beams reinforced with basalt FRP for flexure and shear. J Compos Constr 2015;04014036:1–10. https://doi.org/10.1061/(ASCE)CC.1943-5614.0000491.
[21] Hill RC, Bowen PA. Sustainable construction: principles and a framework for attainment. Constr Manag Econ 1997;15(3):223–39. https://doi.org/10.1080/014461997372971.
[22] Alnahhal W, Taha R, Alnuaimi N, Al-Hamrani A. Properties of fibre-reinforced concrete made with discarded materials. Mag Concr Res 2019;71(3):152–62. https://doi.org/10.1680/jmacr.17.00293.
[23] Al-Hamrani A, Kucukvar M, Alnahhal W, Mahdi E, Onat NC. Green concrete for a circular economy: a review on sustainability, durability, and structural properties. Materials (Basel) 2021;14:1–33. https://doi.org/10.3390/ma14020351.
[24] Sohail MG, Alnahhal W, Taha A, Abdelaal K. Sustainable alternative aggregates: characterization and influence on mechanical behavior of basalt fiber reinforced concrete. Constr Build Mater 2020;255:119365. https://doi.org/10.1016/j.conbuildmat.2020.119365.
[25] Alnahhal W, Taha R, Al-Nasseri H, Nishad S. Effect of using Cement Kiln Dust as a nano-material on the strength of cement mortars. KSCE J Civ Eng 2018;22(4):1361–8. https://doi.org/10.1007/s12205-017-0010-6.
[26] Karsan KR, Hoseini AG. Investigating the effectiveness of using green concrete towards promotion of sustainable built. Univ Putra Malaysia 2015;8:49–59.
[27] Andrew RM. Global CO2 emissions from cement production. Earth Syst Sci Data Discuss 2017:195–217. https://doi.org/10.5194/essd-2017-77.
[28] Kayali O, Ahmed MS. Assessment of high volume replacement fly ash concrete – Concept of performance index. Constr Build Mater 2013;39:71–6. https://doi.org/10.1016/j.conbuildmat.2012.05.009.
[29] Rivera F, Martínez P, Castro J, Mauricio L. Massive volume fl y-ash concrete: a more sustainable material with fl y ash replacing cement and aggregates. Cem Concr Compos 2015;63:104–12. https://doi.org/10.1016/j.cemconcomp.2015.08.001.
[30] Ding J, Li Z. Effects of metakaolin and silica fume on properties of concrete. ACI Mater J 2018;99:393–8.
[31] Shekarchi M, Rafiee A, Layssi H. Long-term chloride diffusion in silica fume concrete in harsh marine climates. Cem Concr Compos 2009;31(10):769–75. https://doi.org/10.1016/j.cemconcomp.2009.08.005.
[32] Saha AK. Effect of class F fl y ash on the durability properties of concrete. Sustain Environ Res 2018;28(1):25–31. https://doi.org/10.1016/j.serj.2017.09.001.
[33] Nath P, Sarker P. Effect of fly ash on the durability properties of high strength concrete. Procedia Eng 2011;14:1149–56. https://doi.org/10.1016/j.proeng.2011.07.144.
[34] Çelik B, Özturan T. Green concrete produced by fly ash and silica fume. Int J Eng Sci Appl 2017;1:1–6.
[35] Khedr SA, Abou-Zeid MN. Characteristics of silica-fume concrete. J Mater Civ Eng 1994;6(3):357–75.
[36] Mazloom M, Ramezanianpour AA, Brooks JJ. Effect of silica fume on mechanical properties of high-strength concrete. Cem Concr Compos 2004;26(4):347–57. https://doi.org/10.1016/S0958-9465(03)00017-9.
[37] Wong HS, Abdul Razak H. Efficiency of calcined kaolin and silica fume as cement replacement material for strength performance. Cem Concr Res 2005;35(4):696–702. https://doi.org/10.1016/j.cemconres.2004.05.051.
[38] Behnood A, Ziari H. Effects of silica fume addition and water to cement ratio on the properties of high-strength concrete after exposure to high temperatures. Cem Concr Compos 2008;30(2):106–12. https://doi.org/10.1016/j.cemconcomp.2007.06.003.
[39] Amudhavalli NK, Mathew J. Effect of silica fume on strength and durability parameters of concrete. Int J Eng Sci Emerg Technol 2012;3:28–35.

[40] Nochaiya T, Wongkeo W, Chaipanich A. Utilization of fly ash with silica fume and properties of Portland cement – fly ash – silica fume concrete. Fuel 2010;89(3): 768–74. https://doi.org/10.1016/j.fuel.2009.10.003.
[41] Lam L, Wong YL, Poon CS. Effect of fly ash and silica fume on compressive and fracture behaviors of concrete 1998;28(2):271–83.
[42] Arezoumandi M, Volz JS, Myers JJ. Effect of high-volume fly ash on shear strength of concrete beams. Transp Res Rec 2013;2342(1):1–9. https://doi.org/10.3141/2342-01.
[43] Rao P, Mohan S, Sekar S. Shear resistance of high volume fly ash reinforced concrete beams without web reinforcement. Int J Civ Struct Eng 2013;1:986–93.
[44] ASTM C39/C39M – 20. Standard Test Method for Compressive Strength of Cylindrical Concrete Specimens. 2020. https://doi.org/10.1520/C0039.
[45] ASTM C1609/C1609M-12. Standard Test Method for Flexural Performance of Fiber-Reinforced Concrete (Using Beam With Third-Point Loading). 2012. https://doi.org/10.1520/C1609_C1609M-12.
[46] ASTM D7205/D7205M-06. Standard Test Method for Tensile Properties of Fiber Reinforced Polymer Matrix Composite Bars. 2016. https://doi.org/10.1520/D7205.
[47] MST-BAR 2017.
[48] American Concrete Institute (ACI) Committee 440. Guide for the Design and Construction of Structural Concrete Reinforced with Fibre-Reinforced Polymer (FRP) Bars (ACI 440.1R-15). 2015. https://doi.org/10.1061/40753(171)158.
[49] CSA (Canadian Standards Association). Design and construction of building components with fiber reinforced polymers. (CSA-S806-12) 2012.
[50] ISIS (Intelligent Sensing for Innovative Structures). Reinforcing Concrete Structures with Fibre Reinforced Polymers; 2007.
[51] JSCE (Japan Society of Civil Engineers). Recommendation for design and construction of concrete structures using continuous fiber reinforcing materials. 1997:1–58.
[52] Alhamad S, Al Banna Y, Al Osman A, Mouthassseeb J. Effect of shear span-to-depth ratio on the shear behavior of BFRP-RC deep beams. MATEC Web Conf 2017; 01012:1–7. https://doi.org/10.1051/matecconf/2017120012.